

1 **Determination of Size Distribution of Precipitation Aggregates Using**
2 **Non-Invasive Microscopy and Semiautomated Image Processing and**
3 **Analysis**

4 Michelle Quilaqueo¹, Minghai Gim-Krumm^{1,2}, René Ruby-Figueroa³, Elizabeth
5 Troncoso^{2,3*}, Humberto Estay^{1*}

6
7
8 ¹Advanced Mining Technology Center (AMTC), University of Chile, Av. Tupper 2007 (AMTC Building),
9 Santiago, Chile.

10 ²Department of Chemistry, Universidad Tecnológica Metropolitana, Las Palmeras 3360, Ñuñoa, Santiago,
11 Chile.

12 ³Programa Institucional de Fomento a la Investigación, Desarrollo e Innovación, Universidad Tecnológica
13 Metropolitana, Ignacio Valdivieso 2409, San Joaquín, Santiago, Chile.

14
15
16 *Corresponding authors:

17 Dr. Humberto Estay, Advanced Mining Technology Center (AMTC), University of Chile,
18 Tupper 2007 (AMTC Building), Santiago, Chile. E-mail: humberto.estay@amtc.cl

19 Dr. Elizabeth Troncoso, Department of Chemistry, Universidad Tecnológica Metropolitana,
20 Las Palmeras 3360, Ñuñoa, Santiago, Chile. E-mail: elizabeth.troncoso@utem.cl

25 **Abstract**

26 Precipitation processes are technologies commonly used in hydrometallurgical plants to
27 recover metals or to treat wastewaters. Moreover, solid-liquid separation technologies, such
28 as thickening or filtering, are relevant unit operations, included in the precipitation
29 technologies. These methods are strongly dependent on the characteristics of the solid
30 precipitates formed during the specific precipitation reaction. One of these characteristics is
31 the particle size distribution (PSD) of the solid precipitates which are fed into a solid-liquid
32 separation process. Therefore, PSD determination is a typical practice for the characterization
33 of the slurries generated in a precipitation plant. Furthermore, the precipitates generated in
34 these processes have a colloidal or aggregation behavior, depending on the operational
35 conditions. Nevertheless, the conventional methods used to estimate PSD (e.g., laser
36 diffraction and/or cicloizer) have not been designed to measure particles that tend to
37 aggregate or disaggregate, since they include external forces (e.g., centrifugal, agitation,
38 pumping and sonication). These forces affect the true size of the aggregates formed in a unit
39 operation, thereby losing representativity in terms of aggregates particle size. This study
40 presents an alternative method of measuring the size distribution of particles with aggregation
41 behavior, particularly, by using non-invasive microscopy and image processing and analysis.
42 The samples used have been obtained from an experimental precipitation process by applying
43 sulfidization to treat the cyanide-copper complexes contained in a cyanidation solution. This
44 method has been validated with statistical tools and compared with a conventional analysis
45 based on laser diffraction. Our results show significant differences between the methods
46 analyzed, demonstrating that image processing and analysis by microscopy is an excellent
47 and non-invasive alternative to obtaining size distribution of aggregates in precipitation
48 processes.

49 **Keywords:** SART process; precipitation aggregates; image analysis; microscopy; particle
50 size distribution

51

52 **1. Introduction**

53 *1.1 Background*

54 The precipitation process is one of the technological options available for treating solutions
55 in hydrometallurgical plants, with the purpose of recovering or removing metals, among
56 others compounds [1]. Typical applications are found in gold cementation, using zinc powder
57 [2]; copper cementation, using scrap iron [1]; acid mine drainage (AMD) treatment, using
58 milk of lime [3]; copper sulfide precipitation from acid mine drainage, using hydrogen sulfide
59 [4]; and copper sulfide precipitation from cyanide solutions in gold mining [5]. These
60 processes must accommodate a subsequent solid-liquid separation stage (i.e., thickeners
61 and/or filters) to remove the solids generated from the solution. The characteristics of these
62 precipitates (colloidal behavior and fine particles) determine the thickeners, large filter size,
63 and rigorous operational control required in order to prevent a high content of suspended
64 solids in the recovered solutions [6-9]. Particularly, the copper sulfide precipitation process
65 from acid mine drainage and cyanide solutions is very attractive, owing to its capacity to
66 recover valuable by-products from wastewaters (in the case of AMD) and gold mining (in
67 the case of cyanide solutions). An appropriate characterization of the precipitate size is
68 crucial for the selection and design of an adequate separation process. In this context, there
69 are some studies that characterize the precipitates formed in sulfidization processes for
70 treating AMD [6,7] and cyanide solutions [9]. These studies determined the aggregate
71 characteristics from metal sulfide precipitates and the dependence of pH and sulfide dosage
72 (chemical solution characteristics) on aggregate size. Thus, settling rate results determined

73 by operational conditions related to pH and sulfide dosage. These results indicate the
74 relevance of the aggregate size to operational conditions when operating and designing solid-
75 liquid separation equipment. For this reason, the experimental technique used to quantify
76 particle size and particle size distribution could play a critical role in the interpretation of
77 data, which may underestimate or overestimate set-points for chosen operational conditions
78 when operating solid-liquid separation equipment. Unfortunately, the methodologies
79 currently used to measure particle size and particle size distribution (PSD) of fine particles
80 (0.1 - 100 μm), such as Malvern Mastersizer (MMS) or cyclosizer (CS), have been designed
81 to quantify PSD, but not to measure aggregate size distribution (ASD). This quantification is
82 crucial when defining optimal operational conditions for thickening process. The two
83 methods mentioned above (MMS and CS) involve external forces (e.g., agitation, pumping
84 and centrifugal in the case of CS) which can affect the physical integrity of the aggregates,
85 and consequently alter their size distribution. A previous study shows the impact of CS on
86 the mineral's surface, owing to the external forces applied to separate particles of different
87 sizes [10]. However, the Focused Beam Reflectance Measurement (FBRM) allows the
88 aggregate size distribution to be determined, although this technique is still very expensive
89 for experimental and research purposes. Hence, it is necessary to quantify the ASD using
90 non-invasive and less expensive techniques than FBRM. In this context, this study proposes
91 a new non-invasive method to quantify size distribution of aggregates using microscopy and
92 semiautomated image processing and analysis.

93

94 ***1.2 Particle size distribution using microscopy and image processing and analysis***

95 The measurement of particle or aggregate size distribution is not a simple task, because it
96 depends on a series of factors which affect the measurement. As mentioned above, these

97 factors include the heterogeneity of the sample itself as well as the strategy employed to make
98 the results representative of the sample's characteristics. In this regard, microscopy is a
99 technique that has not only been used as a powerful tool when morphological information is
100 required to understand the behavior of a material (such as civil engineering materials) [11,12]
101 or in the electronics industry [13], but also to quantify the particle size distribution
102 successfully in various fields, such as food, pharmaceuticals, and mineral processing. For
103 example, microscopy has been employed to quantify microstructures and correlate them with
104 rheological properties in apple tissue [14]. Also, microscopy has been applied to determine
105 the bubble size distribution in aerated whey protein gels [15]. Moreover, successful
106 applications have also been reported regarding the measurement of soil grain-size
107 distribution, in which no significant differences were found in comparison with the traditional
108 mechanical (sieve) analysis [11,16] or the use of reflected light microscopy (RLM) for the
109 recognition of hematite grains in materials engineering [17]. In addition, interesting
110 applications have been reported in batch solution crystallization processes, where images
111 captured by microscopy enabled the estimation of the time-varying particle size distribution
112 of particles in suspension, through crystallization experiments [18]. After using image
113 processing and analysis, it was also possible to determine simultaneous occurrence of
114 particulate events such as nucleation, breakage, and aggregation, in order to monitor and
115 control the properties of crystalline products [18]. In this sense, the application of confocal
116 microscopy and multiple sensors for dynamic measurements of crystal properties, such as
117 size, shape, and polymorph, allows relevant attributes to be determined, related not only to
118 downstream processes (filtration, washing, granulation, drying, grinding, transportation,
119 storage, and tableting), but also to end-use properties, such as bulk density, mechanical
120 strength of a tablet, catalytic activity, stability, wettability, and flowability [19].

121 Consequently, the application of image processing and analysis for aggregate size and shape
122 determinations could be beneficial for the mining , comminution, and materials handling
123 industries. In particular, the efficiency of these technologies is located in their capacity to
124 make measurements without disrupting production streams, as traditional sieving methods
125 do. Additionally, measurements can be made in real time, so that appropriate adjustments to
126 the comminution and screening processes can be made in real time, before large quantities
127 of out-of-specification materials are produced [20].

128 Among the advantages of microscopy over other techniques, is the fact that it is less
129 expensive than the others – in terms of capital costs -and in particular the fact that it makes
130 the particle size and shape visible, without any intervention during the analysis. Its
131 disadvantages, however, mainly relate to the reliability of its measurements, that is, for
132 selecting the representative number of particles measured [14,21,22]. Furthermore, in some
133 cases it is difficult to determine whether two or more particles are “touching” or if they are
134 permanently stuck together and, therefore, must be considered to be one bigger particle [19].

135 In addition, some authors emphasize that the sampling preparation, acquisition, and nature
136 of images, image processing, such as linear filters, rank filters, and morphological filters,play
137 a key role [12]. All of the considerations mentioned are essential in the variability of the
138 measurement. However, there are several statistical tools that one may use to address the
139 disadvantages mentioned above and to validate that the microscopic measurement is
140 representative. In this regard, analysis of the variability between the images per sample and
141 between samples will allow it to be determined whether there are significant differences
142 between the distribution of particles or aggregates size that were measured. Depending on
143 the data distribution (normal distribution or not), parametric and non-parametric statistics can
144 be used to compare the population group (data within images or between images).

145 The aim of this study was to apply a non-invasive method to quantify the size distribution of
146 aggregates using optical microscopy and semiautomated image processing and analysis. This
147 valuable information can be a useful tool for measuring, in a more realistic manner, the
148 aggregate size distribution and the critical parameter when designing optimal operational
149 conditions for the solid-liquid separation processes.

150

151 **2. Methodology**

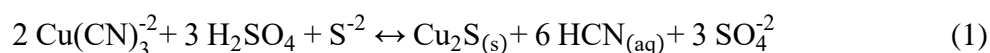
152 **2.1 Reagents**

153 The reagents used in this study (NaCN, CuCN, NaHS, NaOH, and H₂SO₄) were analytical
154 grade chemicals obtained from Merck and Sigma Aldrich. All solutions were made using
155 demineralized water (<1 μS). The pH electrode (Methrom, Model 913) was calibrated using
156 pH buffer solutions (Hanna).

157

158 **2.2 Generation of precipitation aggregates**

159 The precipitation aggregates generated were sulfide copper, which was produced from
160 synthetic cyanide solutions, simulating the typical operational conditions of the SART
161 (Sulfidization, Acidification, Recycling, and Thickening) process. This technology has been
162 designed to recover copper and cyanide from cyanide solutions in gold mining [5,23],
163 according to the following general chemical reaction:



164 The synthetic cyanide solution was made by mixing NaCN, CuCN, and NaOH to adjust the
165 pH value at 12, avoiding HCN volatilization. The copper and total cyanide concentration
166 were fixed at 1800 mg/L and 2460 mg/L, respectively. The copper concentration was chosen

167 based on the copper concentrations found in gold mining, which have high cyanide-soluble
168 copper content in the ore [5,24-26]. Moreover, the cyanide concentration was defined
169 according to the cyanide associated to copper, in order to keep a free cyanide concentration
170 of 100 mg/L; a typical value set in gold mining operations to ensure gold dissolution [2,27].
171 This value was estimated from the thermodynamic equilibrium of the copper-cyanide
172 complexes by using the software Hydra/Medusa from the KTH Royal Institute of Sweden
173 [28] The sulfidization reaction (Equation 1) was carried out in a glass reactor of 650 mL
174 capacity over a period of 15 minutes, setting the pH at 4.0 and sulfide dosage at 120%
175 stoichiometric, using 1 M sulfuric acid and NaHS dosage, respectively. These conditions
176 were selected with the aim of ensuring the maximum precipitate generation according to
177 literature [5].

178

179 *2.2 Size distribution analysis techniques*

180 *2.2.1 Laser diffraction analysis*

181 A 600 mL sample of a suspension which resulted from the sulfide precipitation was analyzed
182 by the laser diffraction technique, using a Malvern Mastersizer 2000 (MM2000). The aim
183 was to measure the particle size distribution (PSD) of the suspended solids (i.e., copper
184 sulfide precipitates). The Mastersizer equipment uses an agitated tank which operates at 1000
185 rpm. The sample is recirculated by a centrifugal pump (2500 rpm), in order to keep the solids
186 suspended and homogenized in the suspension. Additionally, the supplier of the Mastersizer
187 2000 (MM2000) recommends the use of an additional pre-treatment of ultrasound at 20 KHz
188 during 1 minute, during which suspended particles form aggregates [29].

189

190 *2.2.2 Microscopy and semiautomated image processing and analysis*

191 The particle size distribution (PSD) of aggregates was measured using an optical microscope
192 (Leica DM 750) connected to a digital camera HD 5 MGPXL WI-FI (Leica ICC50W), which
193 captured the images. The size distribution estimate was determined using two software for
194 image processing. The Leica Application Suite V4 12 was used to measure the equivalent
195 diameter of the aggregates up to 320 μm , whereas aggregates with an equivalent diameter
196 larger than 320 μm were analyzed using the software Image Pro Plus 6. After these analyses,
197 the complete PSD was estimated by mixing the distribution curves obtained from both
198 software. The image-processing and analysis was carried out using two software, in order to
199 ensure the precision of the measurements in a wide range of diameter sizes.

200 It is crucial that samples are representative, in order to give reliable information for process-
201 control purposes. Taking this issue into account and adding the fact that copper sulfide
202 precipitates tend to form aggregates rapidly, the suspension sampling and the image-capture
203 must be carried out in a short time span. Hence, when the sulfidization reaction was
204 completed (after 15 min), the suspension sampling and image-capture were performed in a
205 maximum time period of two minutes. Samples were taken at the same level of the agitated
206 reactor, using a siringe connected to a 7 mm tubing to avoid the destruction of aggregates. In
207 this time, it was possible to capture nine images (M1 to M9 images), which were obtained
208 from 70 μL of suspension collected from the reactor. These samples were placed on three
209 zones of the microscope slide in order to be analyzed by the optical microscope.

210

211 ***2.3 Measurement of copper content in the sulfide precipitate***

212 The copper sulfide precipitate obtained during the sulfidization reaction was characterized
213 by a scan by an electron microscope coupled with an energy-dispersive X-ray (SEM-EDX),

214 JEOL model IT300 LV. With this analysis, the copper content in the precipitate generated
215 was quantified.

216

217 ***2.4 Copper sulfide conversion***

218 A sample of the suspension was taken from the sulfidization reactor during each 15-min
219 reaction interval. This sample was filtered using a syringe filter of 0.22 μm pore size. The
220 solution collected was neutralized at pH 12 with a 1M NaOH solution. The dissolved copper
221 was measured using an atomic absorption spectrometer (AAS), GBC model SensAA dual.
222 The copper concentration measured in the sample was used to estimate the conversion of
223 sulfide copper precipitate (copper recovery), considering the initial copper concentration in
224 the cyanide solution. Moreover, the total suspended solids (TSS) was estimated using the
225 following equation.

$$\text{TSS} = \frac{\text{Initial copper concentration} \times \text{Copper conversion}}{\text{Copper content}} \quad (2)$$

226 ***2.5 Statistical analysis***

227 For the PSD estimation, data obtained from images captured using optical microscopy (MC)
228 comprised nine images (M1...M9), from which 192 objects were randomly chosen (particles
229 were measured by a proper methodology according to their size, as previously described).
230 Furthermore, the PSD measurements made using the laser diffraction technique (MM2000)
231 were divided into two groups: (i) samples without pre-treatment (MS1) and (ii) samples pre-
232 treated by the use of sonication (MS2). Thus, 556 and 377 objects formed the population of
233 MS1 and MS2, respectively. Then, the first step was to analyze the data distribution (test
234 normal distribution) for the PSD obtained by optical microscopy and laser diffraction
235 technique, for the samples with and without pre-treatment. The exploratory data analysis,

236 which determines whether the data has a normal distribution, is crucial for adequately
237 selecting the parametric or non-parametric statistics. This is because many statistical
238 procedures, including correlation, regression, *t* test and the analysis of variance ANOVA
239 (parametric tests), are based on the assumption that the data follows a normal distribution. In
240 the case of abnormally distributed data, the use of parametric statistics does not allow
241 accurate and reliable conclusions to be drawn [30]. In this regard, the normality was
242 evaluated by two common and robust non-parametric statistics for this purpose:: modified
243 Kolmogorov-Smirnov (K-S) and Shapiro-Wilk (S-W). After determining the data
244 distribution, multiple comparison tests were conducted in order to determine whether there
245 were significant differences between the data obtained by optical microscopy and those
246 obtained by the laser diffraction technique for PSD. From a statistical point of view, these
247 are crucial for guaranteeing that optical microscopy can be used as a valid technique for PSD
248 analysis. In the case of images obtained by microscopy (M1...M9), the comparison was
249 carried out by the analysis of variance ANOVA (parametric test) and Kruskal Wallis, which
250 is the equivalent non-parametric statistic for one-way ANOVA [31]. In cases where ANOVA
251 and Kruskal Wallis reject the null hypothesis, this means that there are significant differences
252 between the PSD on the microscopy images. It is then necessary to perform additional
253 analysis (post-hoc test) to clarify the differences between particular pairs of experimental
254 groups. Tukey's HSD (honestly significant difference) procedure was used as a post-hoc test
255 because it allows multiple comparisons of the mean to be performed, in order to evaluate
256 whether there are significant differences between the means at 95% of confidence level. The
257 same procedure was performed for the data comparison between microscopy and laser
258 diffraction technique, with and without pre-treatment as well as for the validation test using
259 non-agglomerated material as CuCN.

260

261 ***2.6 Validation of method using an unbiased sample***

262 Considering the aggregation behavior of copper precipitates and the effect of time
263 measurement on the PSD, a validation procedure was performed, in order to estimate the
264 error of the method proposed in this study with respect to the MM2000, using an unbiased
265 sample. For this purpose, a sample of an insoluble salt in water without aggregation behavior
266 (CuCN, the same used for synthetic solutions) was used to validate the measure of PSD by
267 microscopy. In this sense, a suspension of 1 g/L of CuCN was prepared using demineralized
268 water. The method of data acquisition by microscopy employed was the same as the method
269 described in section 2.2.2. The statistical procedure employed was the same as the procedure
270 described in section 2.5.

271

272 **3. Results and discussion**

273 ***3.1 Generation of precipitation aggregates***

274 The results of the reaction conversion and the copper content obtained from the sulfidization
275 reaction are shown in Table 1. A maximum precipitate generation of 99.97% was reached for
276 the operational conditions assessed, and it was possible to obtain a precipitate quality with
277 67.69 % w/w of copper content, as found in other SART studies or industrial plants [5]. After
278 determining the copper content and conversion, this data was used to estimate the TSS
279 generated in the reaction, which reached a value of 2,658 mg/L.

280

281 ***3.2 Size distribution analysis***

282 From the distribution curves, the particle size was estimated at 50% distribution (P50) and
283 90% (P90) for all conditions studied (see Table 2). Size data were obtained by laser

284 diffraction using the MM2000 for samples with and without pre-treatment, and by image
285 processing and analysis obtained from samples studied by optical microscopy. The samples
286 pre-treated with sonication (20 kHz), as suggested by the supplier, showed the lowest particle
287 sizes prior to particle size measurement using the MM2000 (6.9 and 17.4 μm for P50 and
288 P90, respectively), in comparison with the samples analyzed by optical microscopy (119 and
289 307 μm , respectively) and the samples analyzed by laser diffraction without sonication (25.7
290 and 59.6 μm , respectively). It is important to mention that the use of sonication is indeed a
291 pre-treatment, as recommended by the supplier. This pre-treatment is carried out with the
292 aim of ensuring good particle size measurements, thereby avoiding aggregation effects in the
293 results. However, the differences observed in the values of particle sizes among the three
294 methods can be explained by the influence of external forces on the samples prior to
295 measuring the particle size, particularly in both cases of MM2000 (agitation, pumping, and
296 sonication). In fact, the sonicated samples presented smaller particle sizes due to
297 disaggregation effects promoted by the sonication, generating fine particles. This
298 methodology can be useful as an informative backup. However, it can yield impractical
299 results for equipment design and process control purposes, since the particles with
300 aggregation behavior will form new aggregates when sonication or other external forces
301 (agitation, pumping) are stopped. Therefore, the results obtained from image analysis
302 captured by optical microscopy are non-invasive. These results can thereby determine more
303 realistic particle sizes of the aggregates. Thus, the P50 size determined by microscopy is
304 around 17 times higher than the MM2000 analysis with pre-treatment, and almost 5 times
305 higher than the MM2000 results without pre-treatment. Figure 1 shows the cumulative size
306 distribution curves obtained with the three methods (MC, MS1 And MS2), where the size
307 distribution resulting from image analysis obtained by microscopy reached values higher

308 than 400 μm , presenting a curve with reduced slope between values 100 and 400 μm . Also,
309 40% of aggregates are smaller than 30 μm in size. Moreover, the disaggregation effect that
310 occurs when using the MM2000 determines a PSD with a high quantity of fine particles.
311 The method of measurement for particle size by optical microscopy was also useful for
312 observing the aggregation evolution over time, specifically when fine particles agglomerate
313 to form new, larger aggregates. In the case of copper sulfide precipitates, the attraction forces
314 promote rapid aggregation among particles. Therefore, the image capture must be very fast.
315 Figure 2 shows the optical micrographs captured by the camera for M1 and M9 samples. In
316 this case, M9 had a higher quantity of aggregates with fewer fine particles around the large
317 aggregates. Figure 3 shows the D50 with respect to the time, from M1 to M9 (at 2 min). The
318 particle size increases drastically from M7, indicating the increase of aggregates, although
319 the behavior in samples M1 to M6 is parabolic, demonstrating a variable behavior. In this
320 context, the validation of the method proposed for measuring particle size distribution is
321 fundamental to support the representativity of the samples taken from a process.

322

323 ***3.3 Statistical analysis of the particle size distribution for copper aggregates***

324 The analysis of size distribution for samples studied by optical microscopy and laser
325 diffraction technique is shown in Table 3. It is appreciated that none of the techniques used
326 for PSD characterization have shown a normal distribution. This is an indication of the
327 complexity of the aggregates and the variability that can be found in the distribution. Figure
328 4 shows the distribution of all the images (M1...M9) in a Box-and-Whisker plot. In this
329 figure not only is it confirmed that the distribution is not normal, but also it is shown that two
330 of the images (M1 and M8) have 50% of the data located in the range of 160-340 μm in
331 comparison with the rest of the images in which 50% of the data are located in a PSD lower

332 than 160 μm . This can be explained by the fact mentioned above, namely, that the precipitates
333 obtained in the sulfidization process tend to aggregate over time. Therefore fewer small
334 particles are quantified by the image analysis during the image capture. The aggregates grow
335 over time, changing the size distribution.

336 According to the non-parametric Kruskal-Wallis, there are significant differences between
337 the images (F-ratio=27.35; p-value=0.0006). Additionally, ANOVA analysis showed that
338 there are significant differences (F-ratio=4.12; p-value=0.0002) between the images
339 (M1...M9) obtained by optical microscopy. However, those differences do not appear in all
340 the images. Figure 5 shows the Tukey's HSD plot for the PSD by optical microscopy, in
341 which it is observed that images M1 and M8 exhibited differences from the other images.
342 The differences observed in these images with respect to the other images can be attributed
343 to the aggregation behavior of precipitates over time. In this case, the M1 image was
344 measured first and M8 was captured closer to the defined time-limit for taking the picture (2
345 min). Therefore, the size of the aggregates is greater than in the other samples. (The 2 min
346 time could be variable for different particles. This will depend on the aggregation
347 characteristics.)

348 Considering that M1 and M8 showed a different distribution, these images were removed
349 from the analysis, since the time that elapsed affected the representativity of these samples,
350 maximizing the size of aggregates with respect to the real-time expended in the reactor.
351 ANOVA and Kruskal-Wallis results without M1 and M8 showed that there are no significant
352 differences between the images for the ANOVA (F-ratio=1.87; p-value=0.0903) and the
353 Kruskal-Wallis test (F-ratio=1.7266; p-value=0.1163). This means that the distribution
354 obtained is representative from a statistical point of view. Additionally, Levene's statistic was
355 calculated in order to determine whether there are significant differences between the

356 standard deviation of the seven images. Results obtained for this statistic showed that there
357 are no significant differences (F-ratio=1.7266; p-value=0.1188) within the standard deviation.
358 Thus, the standard deviation obtained from the seven images is representative at 95% of
359 confidence level.

360 The validated PSD obtained by optical microscopy was compared with the analysis of the
361 laser diffraction technique with and without pre-treatment. ANOVA and Kruskal-wallis
362 analysis showed significant differences between the PSD ($p \leq 0.05$). Figure 6 shows the
363 Tukey's HDS plot in which significant differences between optical microscopy and laser
364 diffraction technique with and without pre-treatment can be observed. It is particularly
365 interesting that the pre-treatment applied to the sample has a significant impact on the PSD.
366 The sample in which a previous sonication (MS2) was applied showed the lower mean of
367 16.2449 μm with a standard deviation of 3.699 μm , whereas the sample without sonication
368 has a mean of 60.226 μm and a standard deviation of 3.046 μm . Considering that PSD plays
369 a crucial role in the solid-liquid separation processes, the type of analysis must be carefully
370 considered, because the pre-treatment and the type of analysis themselves generate variability
371 in the PSD characterization.

372 Furthermore, images obtained by optical microscopy (seven images) showed higher values
373 in the mean (119.721 μm) in comparison with the laser diffraction technique. This result can
374 be explained by the fact that the optical microscopy is not an invasive measurement technique.
375 Therefore, the PSD obtained by optical microscopy represents reality effectively. This is
376 crucial in the selection and design of solid-liquid separation processes. Finally, Figure 7
377 shows the definitive PSD obtained for the six first images ($P_{50}=70 \mu\text{m}$; $P_{90}=190 \mu\text{m}$),
378 comparing it with the MM2000 PSD results. The curve obtained with optical microscopy
379 presents two main zones of particles or aggregates, one representing the fine particles (<70

380 μm) and another one representing the larger aggregates ($>70 \mu\text{m}$). The limit of these two
381 zones and their values of P50 should be the relevant information for use in solid-liquid
382 separation process of precipitates.

383

384 *3.4 Validation of method using an unbiased sample*

385 Results of the comparative analysis for the CuCN sample are shown in Figure 8, where a
386 Tukey's HSD plot for the nine images obtained for CuCN sample is compared with laser
387 diffraction technique measurement (MS). In that Figure, it is observed that there are no
388 significant differences ($p=0.11699$ in ANOVA) between the images (M1...M9) and between
389 them and the laser diffraction technique measurement (MS), as well. This means that
390 microscopy is a validated statistical technique as a non-invasive method for the PSD
391 determination.

392

393 **4. Conclusions**

394 Image processing and analysis using optical microscopy, coupled with statistical methods to
395 validate the results, is a non-invasive and reliable alternative to conventional methods for
396 quantifying the PSD of slurries containing solids with aggregation behavior, generated from
397 precipitation processes. Furthermore, the method presented in this study is easy to implement
398 for research and industrial purposes in a standard laboratory. Additionally, this methodology
399 could also be used to determine PSD for different fine particles (ranging between 1 and 500
400 μm), as an alternative to conventional methods. Therefore, this methodology could be the
401 basis for the application of image processing and analysis to measure PSD in different
402 processes online, in order to improve the control and performance of solid-liquid separation
403 equipment.

404

405 **Acknowledgments**

406 The authors gratefully acknowledge the financial support of the National Commission for
407 Scientific and Technological Research (CONICYT Chile) through the CONICYT-PIA
408 Project AFB180004 and the FONDEF/IDeA Program, FONDEF/CONICYT
409 2017+ID17I10021.

410

411 **References**

- 412 1. Habashi, F. Handbook of Extractive Metallurgy Vol. 1-4, 1997. Wiley-VCH,
413 Weinheim, Germany.
- 414 2. Walton, R. Zinc cementation. In Gold Ore Process, 2nd ed.; Adams, M.D., Ed.;
415 Elsevier. 2016. Amsterdam, The Netherlands, 553–560. [https://doi.org/10.1016/B978-
416 0-444-63658-4.00031-1](https://doi.org/10.1016/B978-0-444-63658-4.00031-1)
- 417 3. Akcil, A., Koldas, S. Acid Mine Drainage (AMD): causes, treatment and case studies.
418 J Clean Prod 2006, 14, 1139-1145. <https://doi.org/10.1016/j.jclepro.2004.09.006>
- 419 4. Fu, F., Wang, Q. Removal of heavy metal ions from wastewaters: A review. J Environ
420 Manage 2011, 92, 3, 407-418. <https://doi.org/10.1016/j.jenvman.2010.11.011>
- 421 5. Estay, H. Designing the SART process – A Review. Hydrometallurgy 2018, 176, 147-
422 [165. https://doi.org/10.1016/j.hydromet.2018.01.011](https://doi.org/10.1016/j.hydromet.2018.01.011)
- 423 6. Mokone, T.P., van Hille, R.P., Lewis, A.E. Effect of solution chemistry on particle
424 characteristics during metal sulfide precipitation. J Colloid Interface Sci 2010, 351,
425 10-18. <https://doi.org/10.1016/j.jcis.2010.06.027>
- 426 7. Mokone, T.P., Lewis, A.E., van Hille, R.P. Effect of post-precipitate conditions on
427 surface properties of colloidal metal sulphide precipitates. Hydrometallurgy 2012,
428 119-120, 55-66. <https://doi.org/10.1016/j.hydromet.2012.02.015>
- 429 8. Martin, A., Fawcett, S., Kulczycki, E., Loomer, D., Al, T., Rollo, A. Application of
430 High-Resolution Microscopy Methods to the Analysis of Fine-Grained and
431 Amorphous Treatment Sludges. Proceedings Tailings and Mine Waste, 2011,
432 Vancouver, BC, Canada, 6-9 November.

- 433 9. Fleming, C.A., Melashvili, M. The SART process: killing the sacred cows. In: XXVIII
434 International Mineral Processing Congress (IMPC 2016), Quebec, 2016, Canada, 11-
435 15 September.
- 436 10. Greet, C.J., Smart, R. st.C. The effect of separation by cyclosizing and
437 sedimentation/decantation on mineral surfaces. *Miner Eng* 1997, 10, 995-1011.
438 [https://doi.org/10.1016/S0892-6875\(97\)00079-4](https://doi.org/10.1016/S0892-6875(97)00079-4)
- 439 11. Arasan, S., Akbulut, S., Hasiloglu, A.S. Effect of particle size and shape on the grain-
440 size distribution using Image analysis. *Int J Civ Struct Eng* 2011, 1, 968-985.
441 doi:10.6088/ijcser.00202010083
- 442 12. Coster, M., Chermant, J.L. Image analysis and mathematical morphology for civil
443 engineering materials. *Cem. Concr. Compos.* 2001, 23, 133–151.
444 [https://doi.org/10.1016/S0958-9465\(00\)00058-5](https://doi.org/10.1016/S0958-9465(00)00058-5)
- 445 13. Ghasemy, A., Rahimi, E., Malekzadeh, A. Introduction of a new method for
446 determining the particle-size distribution of fine-grained soils. *Meas. J. Int. Meas.*
447 *Confed.* 2019, 132, 79–86. <https://doi.org/10.1016/j.measurement.2018.09.041>
- 448 14. Ramírez, C., Troncoso, E., Muñoz, J., Aguilera, J.M. Microstructure analysis on pre-
449 treated apple slices and its effect on water release during air drying. *J. Food Eng.* 2011,
450 106, 253–261. <https://doi.org/10.1016/j.jfoodeng.2011.05.020>
- 451 15. Orrego, M., Troncoso, E., Zúñiga, R.N. Aerated whey protein gels as new food
452 matrices: Effect of thermal treatment over microstructure and textural properties. *J.*
453 *Food Eng.* 2015, 163, 37–44. <https://doi.org/10.1016/j.jfoodeng.2015.04.027>
- 454 16. Graham, D., Rice, S.P., Reid, I. A transferable method for the automated grain sizing
455 of rivergravels. *Water Resour Res* 2005, 41, W07020, 1-12.
456 doi:10.1029/2004WR003868
- 457 17. Alvarez-Iglesias, J.C., Gomes, O., Paciornik, S. Automatic recognition of hematite
458 grains under polarized reflected light microscopy through image analysis. *Min Eng*
459 2011, 24, 1264-1270. <https://doi.org/10.1016/j.mineng.2011.04.015>
- 460 18. Presles, B., Debayle, J., Févotte, G., Pinoli, J.C. Novel image analysis method for in
461 situ monitoring the particle size distribution of batch crystallization processes. *J*
462 *Electron Imaging* 2010, 19(3), 031207. DOI: 10.1117/1.3462800
- 463 19. Singh, M.R., Chakraborty, J., Nere, N., Tung, H.H., Bordawekar, S., Ramkrishna, D.

- 464 Image-Analysis-Based Method for 3D Crystal Morphology Measurement and
465 Polymorph Identification Using Confocal Microscopy. *Crist Growth Des* 2012, 12,
466 3735-3748. DOI: 10.1021/cg300547w
- 467 20. Maerz, N.H. Aggregate sizing and shape determination using digital image processing.
468 Center For Aggregates Research (ICAR) Sixth Annual Symposium Proceedings, 1998,
469 St. Louis, Missouri, April 19-20, 195-203.
- 470 21. Ramírez, C., Young, A., James, B., Aguilera, J.M. Determination of a representative
471 volume element based on the variability of mechanical properties with sample size in
472 bread. *J. Food Sci.* 2010, 75, 516–521. [https://doi.org/10.1111/j.1750-
473 3841.2010.01805.x](https://doi.org/10.1111/j.1750-3841.2010.01805.x)
- 474 22. Ramírez, C., Aguilera, J.M. Determination of a representative area element (RAE)
475 based on nonparametric statistics in bread. *J. Food Eng.* 2011, 102, 197–201.
476 <https://doi.org/10.1016/j.jfoodeng.2010.08.021>
- 477 23. MacPhail, P.K., Fleming, C., Sarbutt, K. Cyanide Recovery by the SART Process for
478 the Lobo-Marte Project, Chile. *Randol Gold and Silver Forum*, 1998, Denver (April
479 26-29).
- 480 24. Botz, M., Acar, S. Copper Precipitation and Cyanide Recovery Pilot Testing for the
481 Newmont Yanacocha Project. In: *Society for Mining, Metallurgy & Exploration (SME)*
482 *Annual Meeting*, Denver, 2007, February, 25–28.
- 483 25. Botz, M., Kaczmarek, A., Orser, S. Managing copper in leach solution at the Copley
484 gold mine: laboratory testing and process design. *Miner Metall Proc* 2011, 28, 133-
485 138. DOI: 10.1007/BF03402245.
- 486 26. Estay, H., Carvajal, P., Hedjazi, F., Van Zeller, T. The SART process experience in
487 the Gedabek plant. In: *HydroProcess, 4th International Workshop on Process*
488 *Hydrometallurgy*, 2012, Santiago, Chile.
- 489 27. Marsden, J.O., House, C.I. *The Chemistry of Gold Extraction*. Second ed., Society for
490 *Mining, Metallurgy and Exploration SME*, 2006, Colorado, USA.
- 491 28. Puigdomenech, I. *Hydra-Medusa Software (Hydrochemical Equilibrium Constant,*
492 *Database and Make Equilibrium Diagrams Using Sophisticated Algorithms)*, version
493 1; *Inorganic Chemistry*, 2004. Royal Institute of Technology: Stockholm, Sweden.
- 494 29. Malvern Instruments Ltd. *Mastersizer 2000 User Manual UK*. 2007.

- 495 https://www.labmakelaar.com/fjc_documents/mastersizer-2000-2000e-manual-
496 [eng1.pdf](https://www.labmakelaar.com/fjc_documents/mastersizer-2000-2000e-manual-eng1.pdf).(Accessed 23 November 2018).
- 497 30. Ghasemi, A., Zahediasl, S. Normality tests for statistical analysis: A guide for Non-
498 statisticians. Int J Endocrinol Metab 2012, 10(2), 486-489. doi: 10.5812/ijem.3505
- 499 31. Montgomery, D.C. Design and analysis of experiments-second edition. 2001, Qual.
500 Reliab. Eng. Int. <https://doi.org/10.1002/qre.4680030319>
501

502 **Figure Captions**

503

504 **Figure 1.** Cumulative particle size distribution curve for different methods of particle size
505 measurement. In the case of MC, it considers 9 original samples.

506

507 **Figure 2.** Optical micrographs of samples analyzed at different times, M1 at 10 seconds (left),
508 M9 at 2 minutes (right).

509

510 **Figure 3.** Results of D50 particle size of copper precipitates with respect to the capture time
511 of image in the microscope.

512

513 **Figure 4.** Box-and-Whisker plot for the PSD of nine images obtained by optical microscopy.

514

515 **Figure 5.** Tukey's HDS plot for PSD by optical microscopy.

516

517 **Figure 6.** Tukey's HDS plot for comparison of PSD between optical microscopy and laser
518 diffraction technique with and without pre-treatment.

519

520 **Figure 7.** Cumulative particle size distribution curves for three methods of particle size
521 measurement. In this case, the PSD obtained from image analysis by optical microscopy
522 includes only M1 to M6.

523

524 **Figure 8.** Tukey's HDS plot for comparison of PSD between optical microscopy
525 (M1...M9) and laser diffraction technique (MS) for the CuCN sample.

526

527

528 **List of tables**

529

530 **Table 1.** Sulfidization results.

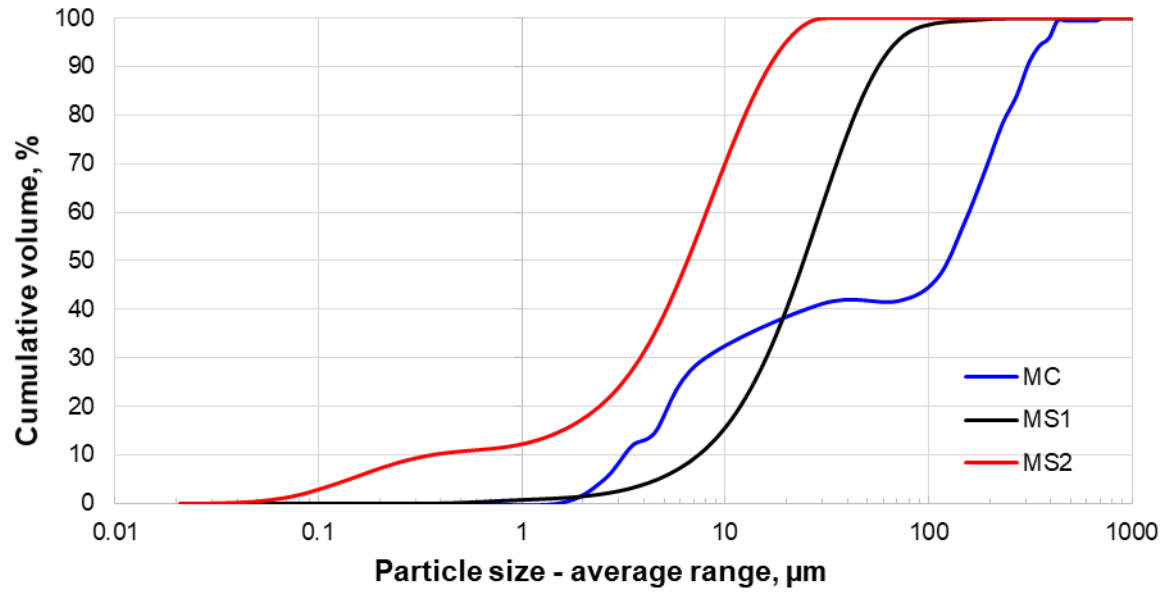
531

532 **Table 2.** Particle size estimated by optical microscopy and laser diffraction technique.

533

534 **Table 3.** Analysis of normal distribution for samples analyzed by optical microscopy and
535 laser diffraction technique.

536

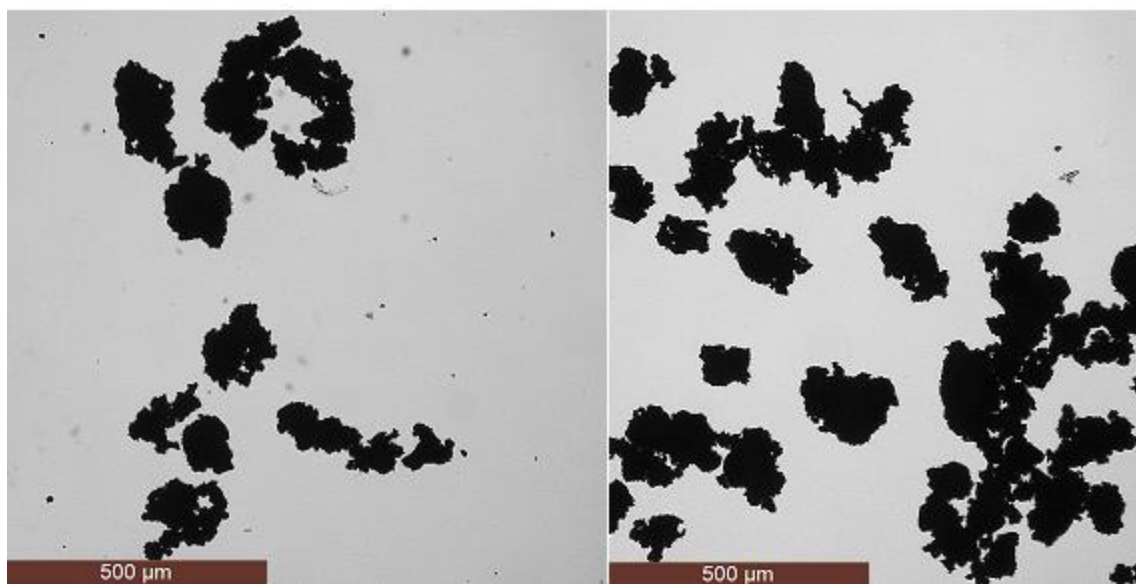


537

538 **Figure 1.** Cumulative particle size distribution curve for different methods of particle size
539 measurement. In the case of MC, it considers 9 original samples.

540

541



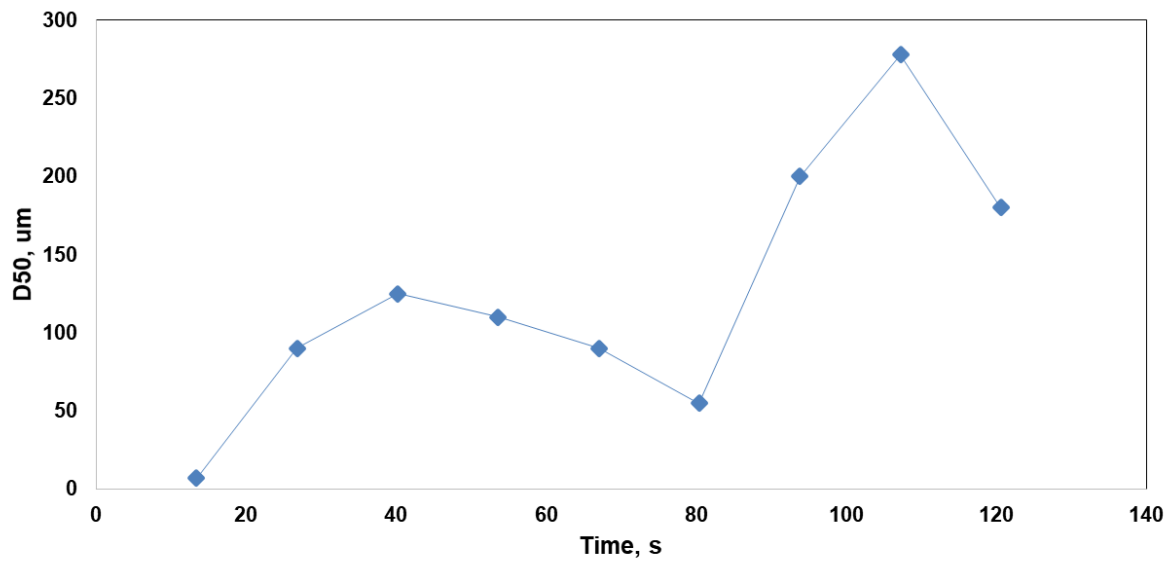
542

543 **Figure 2.** Optical micrographs of samples analyzed at different times, M1 at 10 seconds (left),

544 M9 at 2 minutes (right).

545

546



547

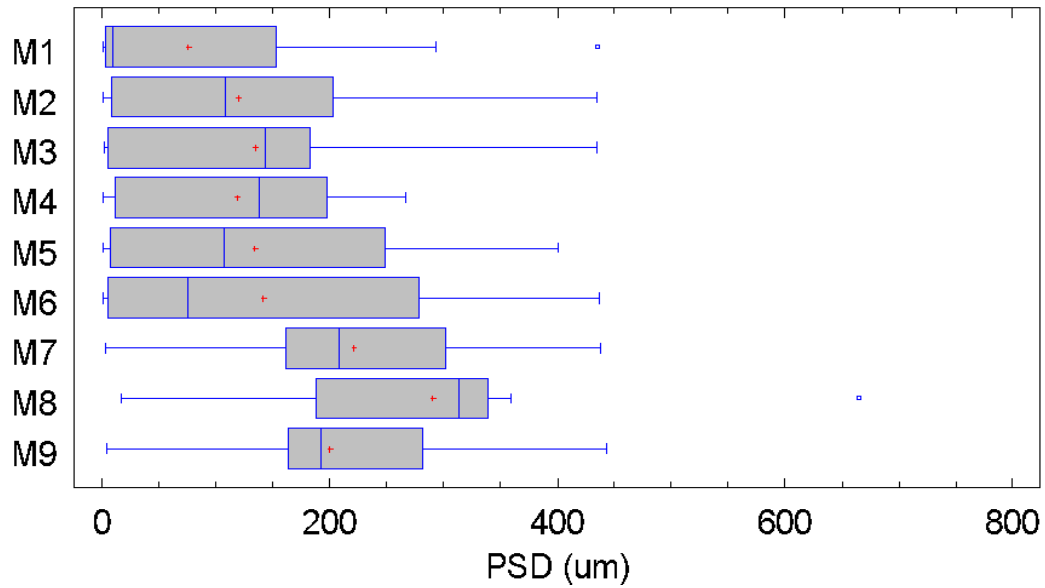
548 **Figure 3.** Results of D50 particle size of copper precipitates with respect to the capture time

549 of image in the microscope.

550

551

552

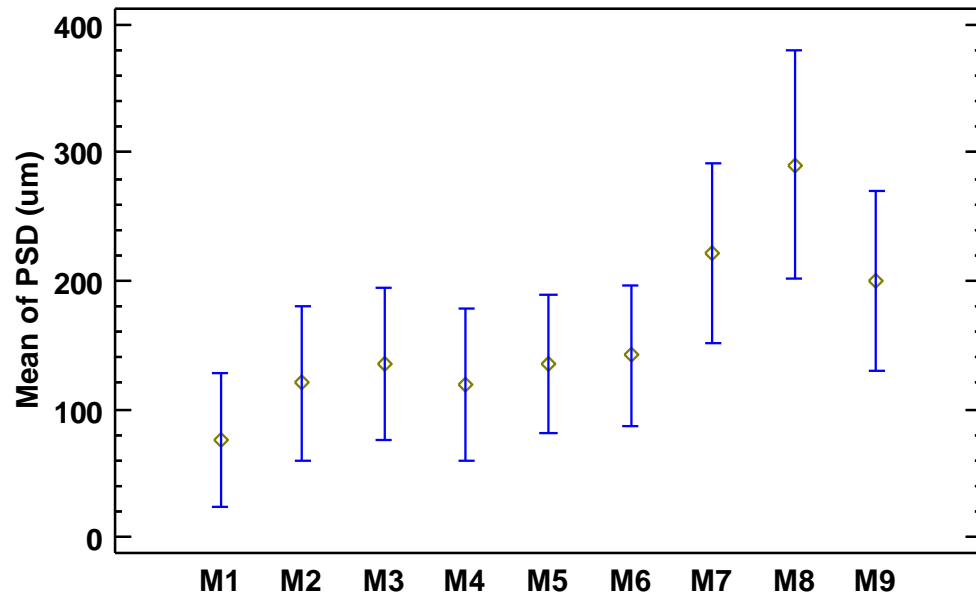


553

554 **Figure 4.** Box-and-Whisker plot for the PSD of nine images obtained by optical microscopy.

555

556

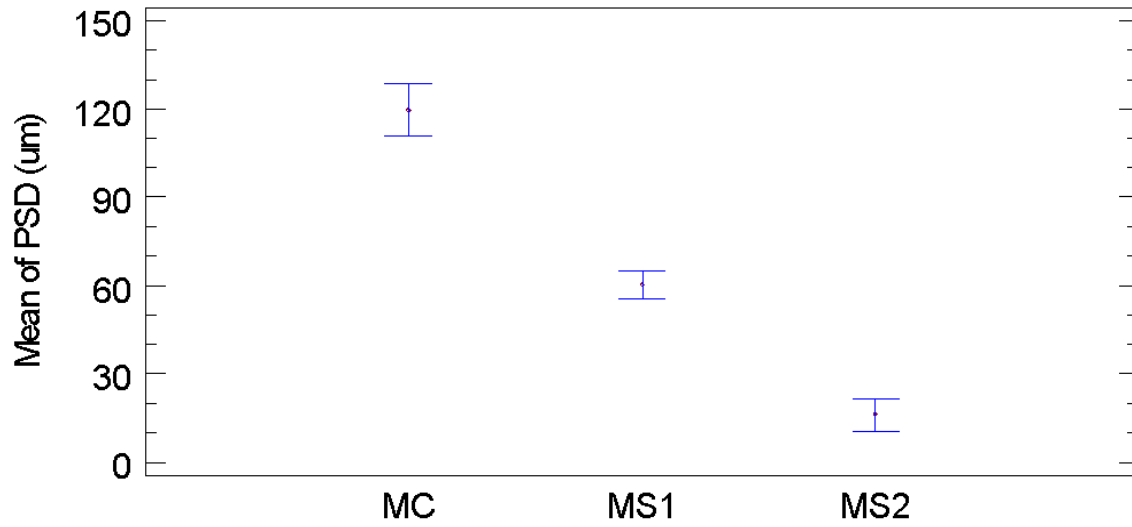


557

558 **Figure 5.** Tukey's HSD plot for PSD by optical microscopy.

559

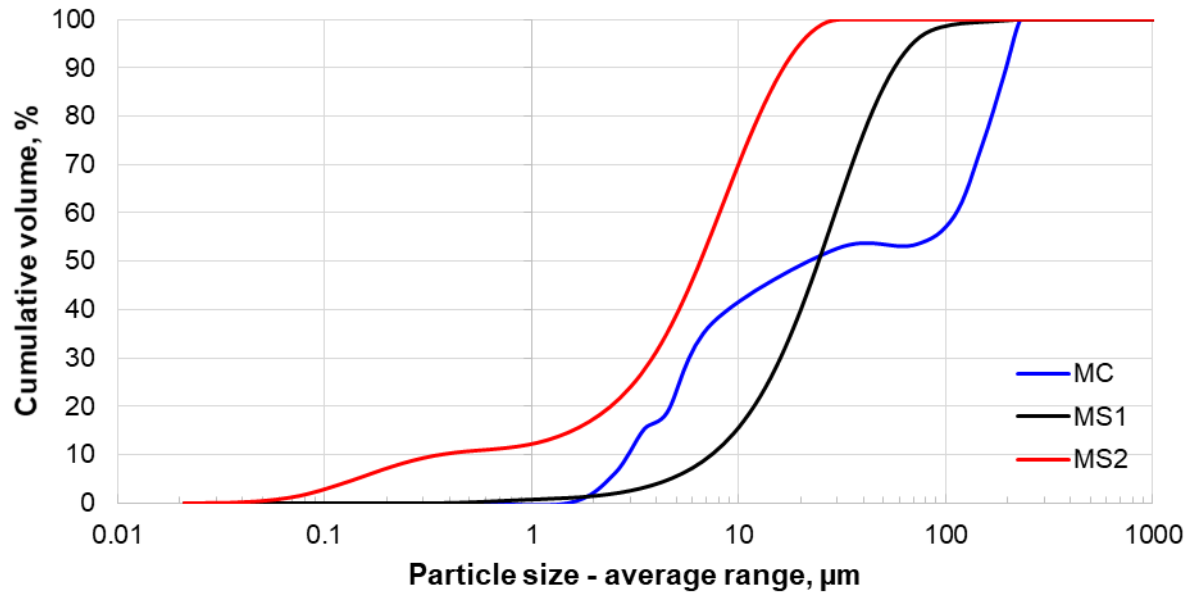
560



561

562 **Figure 6.** Tukey's HSD plot for comparison of PSD between optical microscopy and laser
563 diffraction technique with and without pre-treatment.

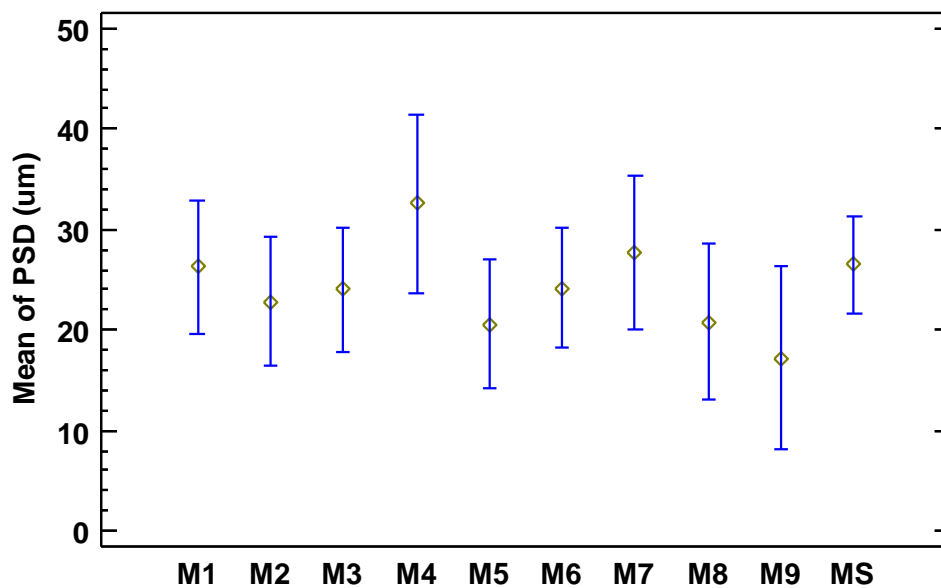
564



565

566 **Figure 7.** Cumulative particle size distribution curves for three methods of particle size
567 measurement. In this case, the PSD obtained from image analysis by optical microscopy
568 includes only M1 to M6.

569



570

571 **Figure 8.** Tukey's HSD plot for comparison of PSD between optical microscopy (M1...M9)

572 and laser diffraction technique (MS) for the CuCN sample.

573

574
575

Table 1. Sulfidization results.

Description	Value
Copper content, % w/w	67.69
Copper sulfide conversion, %	99.97
Total suspended solids, mg/L	2,658

576

577 **Table 2.** Particle size estimated by optical microscopy and laser diffraction technique.

Particle size, μm	MC	MS1	MS2
P50	119	25.7	6.9
P90	307	59.6	17.4

P50: Particle size at 50% distribution; P90: Particle size at 90% distribution.
MC: Optical microscopy; MS1: Laser diffraction without pre-treatment;
MS2: Laser diffraction with pre-treatment.

578

579

580 **Table 3.** Analysis of normal distribution for samples analyzed by optical microscopy and
 581 laser diffraction technique.

Statistics	MC		MS1		MS2	
	F-ratio	p-value	F-ratio	p-value	F-ratio	p-value
Shapiro-Wilk	0.87288	<0.05	0.60841	<0.05	0.77999	<0.05
Modified Kolmogorov-Smirnov	2.73516	<0.05	5.82743	<0.05	5.03322	<0.05

MC: Optical microscopy; MS1: Laser diffraction without pre-treatment.; MS2: Laser diffraction with pre-treatment.

582